AIAA 2002-3033

Progress in the Operation of the Boeing/AFOSR Mach-6 Quiet Tunnel

Steven P. Schneider, Shin Matsumura, Shann Rufer,
Craig Skoch, and Erick Swanson
School of Aeronautics and Astronautics
Purdue University
West Lafayette, IN 47907-1282 USA

22nd AIAA Aerodynamic Measurement Technology and Ground Testing Conference

24–26 June 2002
St. Louis, MO

Progress in the Operation of the Boeing/AFOSR Mach-6 Quiet Tunnel

Steven P. Schneider*, Shin Matsumura†, Shann Rufer‡, Craig Skoch§, and Erick Swanson¶
School of Aeronautics and Astronautics
Purdue University
West Lafayette, IN 47907-1282

Abstract

Purdue University continues to develop a 9.5-inch Mach-6 Ludwieg tube for quiet-flow operation to high Reynolds number. The design, fabrication, and initial operation were reported earlier. The present paper reports progress in achieving and characterizing the quiet Mach-6 flow, and in developing instrumentation. A new design for the bleed-slot throat geometry enabled achieving some initial quiet flow, although only at very low Reynolds numbers of about 200,000. A thicker hot wire of 0.0002-inch diameter is successfully surviving many tunnel runs. Preliminary measurements were obtained on the Hyper2000 generic scramjet forebody using temperature-sensitive paint. These show the development of streamwise vortices from the leading edge imperfections. These vortices become much more evident following the first compression corner, and can be generated in a controlled fashion using small roughness strips on the leading edge.

Introduction

Hypersonic Laminar-Turbulent Transition

Laminar-turbulent transition in hypersonic boundary layers is important for prediction and control of heat transfer, skin friction, and other boundary layer properties. However, the mechanisms leading to transition are still poorly understood, even in low-noise environments. Applications hindered by this lack of understanding include reusable launch vehicles such as the X-33 [1], high-speed interceptor missiles [2], hypersonic cruise vehicles [3], and ballistic reentry vehicles [4].

Many transition experiments have been carried out in conventional ground-testing facilities over the past 50 years. However, these experiments are contaminated by the high levels of noise that radiate from the turbulent boundary layers normally present on the wind tunnel walls [5]. These noise levels, typically 0.5-1% of the mean, are an order of magnitude larger than those observed in flight [6, 7]. These high noise levels can cause transition to occur an order of magnitude earlier than in flight [5, 7]. In addition, the mechanisms of transition operational in small-disturbance environments can be changed or bypassed altogether in high-noise environments; these changes in the mechanisms change the parametric trends in transition [6].

For example, linear instability theory suggests that the transition Reynolds number on a 5 degree half-angle cone should be 0.7 of that on a flat plate, but noisy tunnel data showed that the cone transition Reynolds number was about twice the flat plate result. Only when quiet tunnel results were obtained was the theory verified [8]. Clearly, transition measurements in conventional ground-test facilities are generally not reliable predictors of flight performance.

Development of Quiet-Flow Wind Tunnels

Only in the last two decades have low-noise supersonic wind tunnels been developed [5, 9]. This development has been difficult, since the test-section wall boundary-layers must be kept laminar in order to avoid high levels of eddy-Mach-wave acoustic radiation from the normally-present turbulent boundary layers. A Mach 3.5 tunnel was the first to be successfully developed at NASA Langley [10]. Lan-

*Associate Professor. Associate Fellow, AIAA.
†Research Assistant. Student Member, AIAA.
‡Research Assistant. Student Member, AIAA.
§Research Assistant. Student Member, AIAA.
¶Research Assistant. Student Member, AIAA.

gley then developed a Mach 6 quiet nozzle, which was used as a starting point for the new Purdue nozzle [11]. Unfortunately, this nozzle was removed from service due to a space conflict. Langley also attempted to develop a Mach 8 quiet tunnel [9]; however, the high temperatures required to reach Mach 8 made this a very difficult and expensive effort. This tunnel was officially shut down in early 2001; quiet flow was not achieved and prospects for eventual success were judged poor (Steve Wilkinson, private communication, 2000). The new Purdue Mach-6 quiet flow Ludwieg tube may become the only operational hypersonic quiet tunnel in the world, at least until the old Langley Mach-6 nozzle is brought back online.

Background of the Boeing/AFOSR Mach-6 Quiet Tunnel

A Mach-4 Ludwieg tube was constructed at Purdue in 1992, using a 4-inch nozzle of conventional design that was obtained surplus from NASA Langley. By early 1994, quiet-flow operation was demonstrated at the low Reynolds number of about 400,000 [12]. Since then, this facility has been used for development of instrumentation and for measurements of instability waves under quiet-flow conditions (e.g., Ref. [13, 14, 15]). However, the low quiet Reynolds number imposes severe limitations; for example, the growth of instability waves under controlled conditions on a cone at angle of attack was only about a factor of 2 [16]. This is far smaller than the factor of $e^9 - e^{11}$ typically observed prior to transition, and small enough to make quantitative comparisons to computations very difficult.

A facility that remains quiet to higher Reynolds numbers was therefore needed. The low operating costs of the Mach-4 tunnel had to be maintained. However, hypersonic operation was needed in order to provide experiments relevant to the hypersonic transition problems described earlier. Operation at Mach 6 was selected, since this is high enough for the hypersonic 2nd-mode instability to be dominant under cold-wall conditions, and high enough to observe hypersonic roughness-insensitivity effects, yet low enough that the required stagnation temperatures do not add dramatically to cost and difficulty of operation. Reference [17] describes the overall design of the facility, and the detailed aerodynamic design of the quiet-flow nozzle, carried out using the e^N method. A detailed aerodynamic design of the contraction was also carried out [18]. Reference [18] also supplies a preliminary report on the detailed mechanical design of the nozzle and contraction. Reference [19] reported on design and testing of some of the component parts, including the driver-tube heating, the as-measured contraction contour, the throat-region mandrel fabrication and polishing experience, and so on.

Ref. [20] reports on the design and fabrication of the support structure, diffuser, and second-throat section (which also serves as the sting support). It also reports experience with final contraction fabrication, and with operation of the vacuum system. Ref. [20] also reports on the contour measurements on the third attempt at throat-mandrel fabrication, which completed polishing with good success. Ref. [21] reports (1) the nozzle fabrication, including some of the wall-contour measurements, (2) the contraction-region heating apparatus, (3) the burst-diaphragm tests, (4) the bleed-slot suction system, (5) the electroformed throat properties, and (6) initial hot-wire calibrations.

Ref. [22] reports the rest of the measurements of the as-fabricated nozzle, including initial measurements of tunnel performance. The mean flow and fluctuations were measured in the centerplane using fast pressure transducers (cp. Ref. [12]). Ref. [23] reported on progress in tunnel shakedown and instrumentation development, including efforts to achieve the desired quiet flow by modifying the geometry of the bleed-slot throat, and initial attempts to measure the stagnation temperature in the flow using cold wires. Ref. [24] reported the stress-analysis and testing of the initial conformal window, fabricated in 2001. The present tunnel name was adopted in Spring 2001.

The Boeing/AFOSR Mach-6 Quiet Tunnel

Quiet facilities require low levels of noise in the inviscid flow entering the nozzle through the throat, and laminar boundary layers on the nozzle walls. These features make the noise level in quiet facilities an order of magnitude lower than in conventional facilities. To reach these low noise levels, conventional blow-down facilities must be extensively modified. Requirements include a 1 micron particle filter, a highly polished nozzle with bleed slots for the contraction-wall boundary layer, and a large settling chamber with screens and sintered-mesh plates for noise-reduction [5]. To reach these low noise levels in an affordable way, the Purdue facility has been designed as a Ludwieg tube [12]. A Ludwieg tube is a long pipe with a converging-diverging nozzle on the end, from which flow exits into the nozzle, test section, and second throat (Figure 1). A diaphragm is placed downstream of the test section. When the

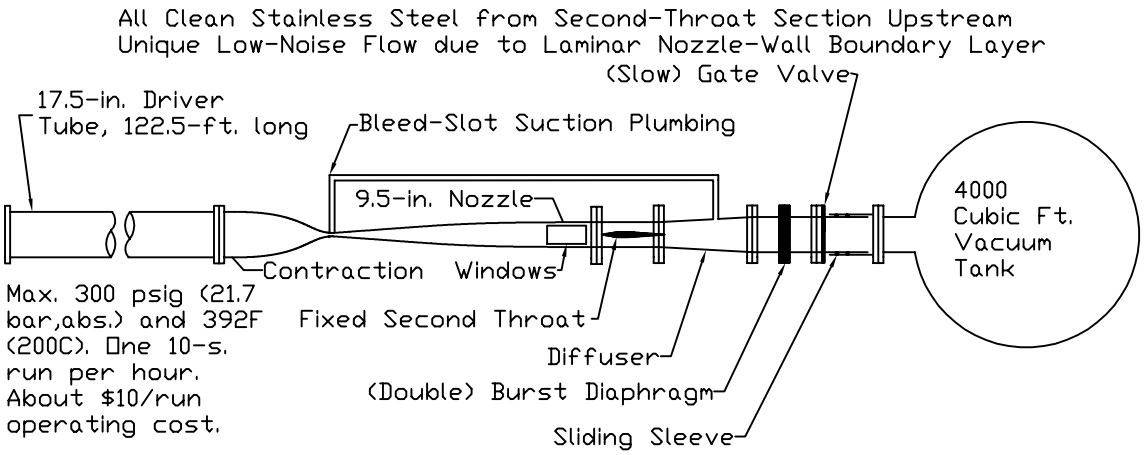

Figure 1: Schematic of Boeing/AFOSR Mach-6 Quiet Tunnel

diaphragm bursts, an expansion wave travels upstream through the test section into the driver tube. Since the flow remains quiet after the wave reflects from the contraction, sufficient vacuum can extend the useful runtime to many cycles of expansion-wave reflection, during which the pressure drops quasi-statically.

Figure 2 shows the nozzle of the new facility. The region of useful quiet flow lies between the characteristics marking the onset of uniform flow, and the characteristics marking the upstream boundary of acoustic radiation from the onset of turbulence in the nozzle-wall boundary layer. The onset of turbulence is drawn for several computational predictions, although quiet flow has not yet been achieved except at very low Reynolds numbers. A 7.5-deg. sharp cone is also drawn on the figure.

Progress with the Probe Traversing Mechanism

The test section traverse system has recently been improved (see Ref. [23] for a description of the original system). Some of the hardware was redesigned to correct galling problems with the probe-support rods. The traverse control software and input/output connections have been updated to allow for external triggering of the probe motion and for triggering an oscilloscope from the probe motion.

The probe support rods had been binding up in the sliding bars, probably due to friction with the O-ring seals, misalignment or bending of the rods, and warping of the original bronze sliding bars. Therefore, a new support system has been designed and built. It includes self-aligning linear bearings to guide the probe support rods and wiring tube. The bearings are housed in a new, stainless-steel top sliding bar. Hydraulic-shaft seals replace the O-rings previously used to seal the rod and tube passages. A larger central tube is used to convey wiring out of the tunnel. This tube is sealed at the top (outside the tunnel) with a Conax probe seal. New Kulite and hot wire probes have been built for use with the new system. The slider-bar clamping-block design has also been updated.

The stepper motor and its control system have been tested and are now operational. Commands are sent from a PC, either in manual mode or through an automated program. Software has been written to enable the traverse to trigger from an external signal, such as the initial pressure drop in the tunnel. System operation has been verified using an external trigger from a function generator. The control software has also been updated to send a probe moving/not-moving signal to an oscilloscope. This has not yet been successfully tested.

In the near future, a triggering system connecting an oscilloscope to the traverse control box will be developed to allow triggering from the initial pressure drop at tunnel start-up. The motion of the probe will be verified using a telescope and reticle and a tunnel test-section reference jig. A feedback loop in which an encoder measures the travel of the linear positioner and conveys this information to a computer will be developed. This will provide an independent measurement of the location of the probe in the tunnel and will potentially allow for on-the-fly motion adjustments.

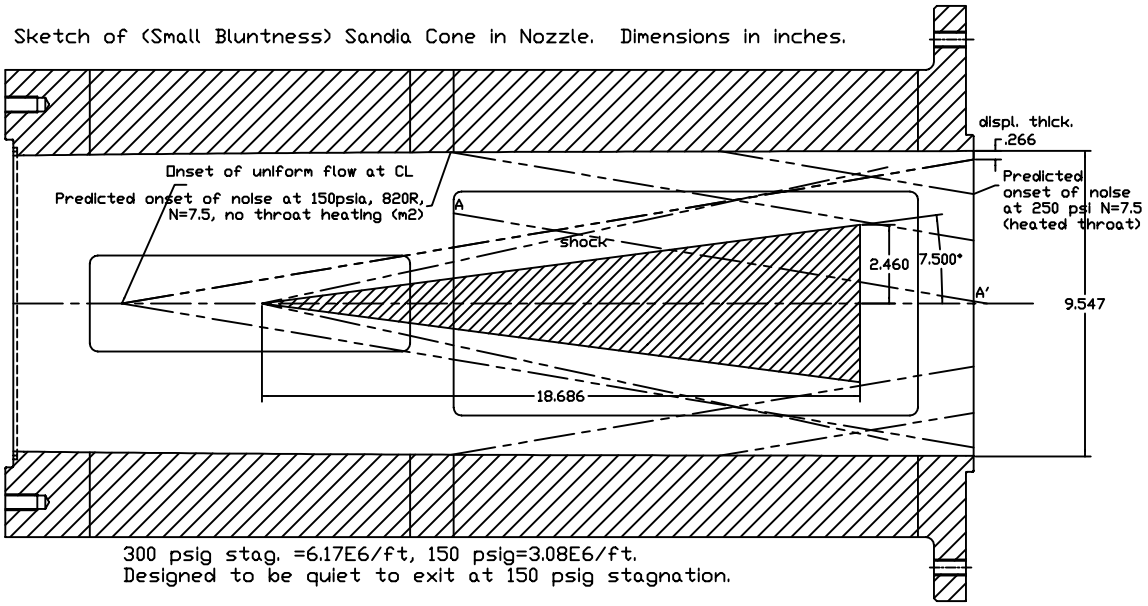

Figure 2: Schematic of Mach-6 Quiet Nozzle with Model

Hot-Wire Instrumentation

Improvements in our calibration methods are currently underway, with measurements to be carried out both in the Mach-6 Ludwieg tube and in a 1-inch jet at about Mach 3.5. The hot-wires are to be calibrated in the 1-inch jet, which was recently modified to achieve less noisy flow. The jet was modified to improve the contraction and add a sintered-metal plate in the settling chamber to reduce valve noise. The stagnation temperature and pressure can be controlled independently in the jet, which should allow reliable calibrations down to the low Reynolds numbers observed in the Mach-6 tunnel. The Mach-number independence principle of hot-wire operation may also be tested, using a second nozzle with a higher Mach number.

Because of the small size and sensitivity of hot wires, they are very easily broken in wind-tunnel runs. For this reason, the hot wires have been tested at various tunnel pressures and temperatures to verify that they will survive the start-up, run, and shut-down conditions in the tunnel. The tests were all conducted using a Purdue-built constant-current anemometer that supplies 2.5 mA from a REF01 IC and amplifies the cold-wire voltage using INA103 IC's. The data were acquired on a LeCroy oscilloscope at 10 kHz for 20 sec. The sampled data were averaged over running intervals of 11 points to reduce the high frequency noise. For each of these runs, the wire was placed very near to the centerline of the tunnel, at about $z = 89$ inches.

The hot-wire probes were specially fabricated following earlier JPL designs to provide minimal blockage in boundary-layer measurements. The assistance of Jim Kendall in this regard has been greatly appreciated. The needles are mounted to a piece of razor blade on the end of a 0.030-inch wide strut that is about 3/4-inch long. The wire is welded onto the two needles, which have a tip diameter of 0.003 in. A slight bow is left in the wire to avoid strain and excess vibrations on the wire during a test.

The first wires tested were Platinum/10% Rhodium (Pt/Rh), with a diameter of 0.0001 in., a typical length/diameter ratio of 300-350, and a cold resistance of 30-35 ohms. These broke repeatedly during shut-down of the tunnel [23]. When the wire was placed on the centerline of the tunnel and no model was in place, the wire survived at most 3 runs at very low pressures, near 1 atm. stagnation. The wire broke during shut-down for every run at higher pressures, above 30 psig.

To address this problem, a thicker Pt/Rh wire was built; this had a diameter of 0.0002 in., a length/diameter ratio of 100, and a cold resistance of about 6 ohms. Six tests were run using this wire, two at atmospheric pressure, one at 46 psia, one at 77 psia, one at 104 psia, and one at 132 psia. The wire survived all six tests, followed by 11 more, for a total of 17, before breaking at the end of a run during tunnel shutdown.

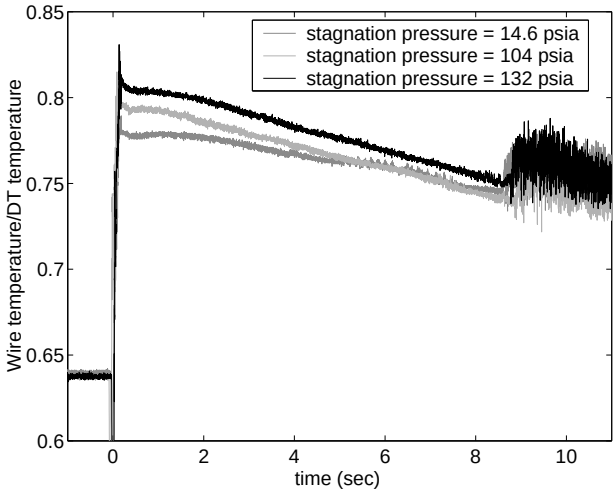

Figure 3: Cold Wire Traces

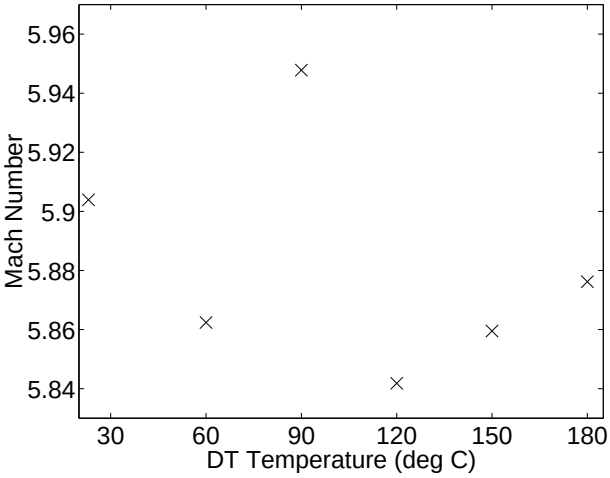

Figure 4: Mach Number vs. Driver Tube Temperature

Figure 3 shows cold-wire traces for the runs at 14.6, 104 and 132 psia. All the runs were made with a driver temperature of approximately 420K. The wire temperature is calculated using the oven calibration, normalized by the initial driver-tube temperature, and plotted against time, where $t = 0$ at the beginning of the run, and the run ends at about $t = 9$ sec. The temperature of the wire at $t < 0$ does not equal that of the driver temperature because only the driver and contraction sections of the tunnel are heated, while the section where the hot wire is located remains near room temperature. The figure shows that the ratio of wire temperature to driver temperature increases with increasing pressure, indicating an increase in recovery factor with increasing Reynolds number. It is not known why the slope of the 14.6-psia curve does not match that of the higher-pressure curves. Future plans include more work in the calibration jet, and tunnel tests of intermediate wire diameters and length/diameter ratios.

Effect of Driver Tube Temperature on Noise

The driver-tube and contraction temperatures were varied to examine the effect that stagnation temperature has on tunnel noise. Runs were performed at approximately 30 deg. C increments, ranging from room temperature to 180 deg. C. Initially, condensation effects were expected for the lower temperatures, but as reported in Ref. [23] they have not yet been observed. All of the runs had a stagnation pressure within 0.2% of 80.8 psia. The measurements were made using a 0-15 psia mechanically-stopped Kulite pressure transducer (XCQ-062-15A) placed on the tunnel centerline at $z = 84.0$ in. Dry air was used, with an estimated dewpoint of -20 deg. C (based on later measurements after a dewpoint meter was installed), and the driver-tube air was allowed to equilibrate for a half hour before each run. The Mach number as a function of driver tube temperature is shown in Figure 4. There does not appear to be any systematic variation of Mach number with driver tube stagnation temperature, but there is some scatter with a difference of 1.8% between the high and low Mach numbers. This is somewhat unexpected as the Mach number should change when the temperature is low enough for nitrogen condensation to occur.

Although temperature has no effect on Mach number, Figure 5 shows that there is definitely an increase of freestream noise as the stagnation temperature is increased. The RMS pitot fluctuations are plotted as a percentage of the mean. All of the RMS values calculated were above the quiet-tunnel limit of 0.1%, but the noise decreases by a factor of about 4 as the driver-tube temperature decreases from $180°C$ to $20°C$. The cause of this remains unexplained, although it is doubtless associated with a reduction in the radiation from the turbulent boundary layer on the nozzle wall. The authors are not aware of any published literature in which this effect is explicitly described, although it may be implicit in previously-published correlations to the boundary-layer properties [25, 26]. Since the reduction in noise is not sufficient to make the tunnel quiet, it is mainly of interest in analyzing

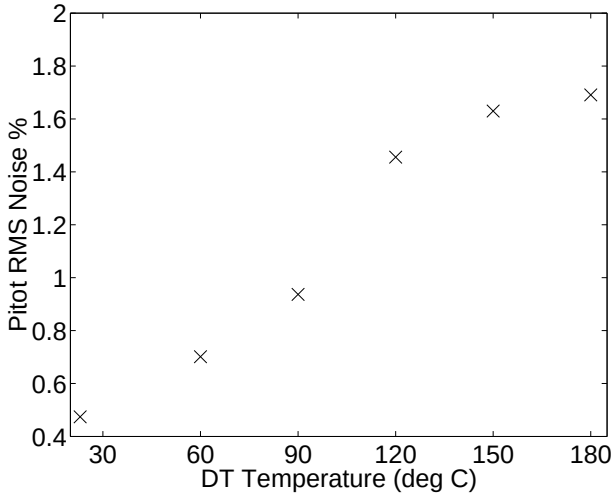

Figure 5: Pitot Fluctuations vs. Driver Tube Temperature

conventional-tunnel measurements of transition. It is evident that such measurements should be expected to contain not only unit-Reynolds number effects due *in part* to changes in nozzle-wall noise radiation, but also tunnel-temperature effects due *in part* to the same effect.

Blockage Tests

Sharp Cone at Zero Angle of Attack

Runs were made with a 7-deg. half-angle sharp blockage cone at nominal initial driver-tube pressures of approximately 120 psig and temperatures of approx. 160 deg. C. Base diameters of 4, 4.5, 4.75, 5.5, and 5.75 inches were used. Figs. 6 and 7 show pitot traces for the 4 and 5.75-inch base-diameter cones. The probe was within about 1 inch from the surface for all of the runs, about 14 inches aft of the cone tip. A Taylor-Maccoll solution for a 7-deg. sharp cone shows that this places the probe behind the shock. The diaphragm breaks at about 0.0 sec., after which there is about 0.2 sec. of startup, followed by near-constant flow conditions. The transducer diaphragm is mechanically stopped so that it reads a maximum of 18 psia prior to the run, although the stagnation pressure is much higher.

The pitot pressure during the run is about 6 psia. The theoretical pitot-pressures behind the shock were calculated based on the Taylor-Maccoll solution, with a conical and isentropic flow behind the shock and no boundary layer. The freestream

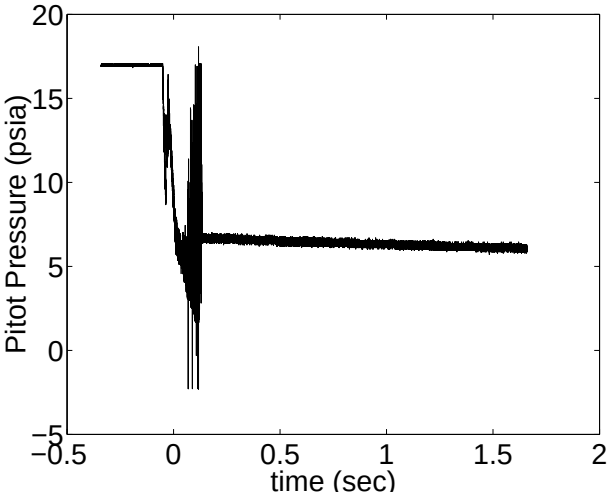

Figure 6: Pitot Measurements Above Cone with 4-inch Base Diameter

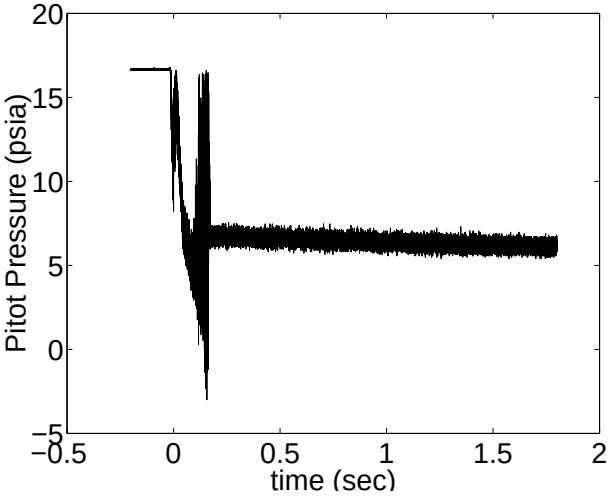

Figure 7: Pitot Measurements Above Cone with 5.75-inch Base Diameter

Mach number was taken as 5.8 and the cone angle was 7 deg. The calculation predicts pitot pressures that increase from 6.67 psia to 7.36 psia, for locations ranging from the shock to the cone surface. The experimental results are slightly lower than the theoretical, indicating some losses, perhaps due to viscous effects. The probe was always at least 0.25 in. from the surface of the cone, and no corrections were made for probe misalignment.

The RMS noise was computed from the pitot fluctuations, normalized by the pitot pressure, and then multiplied by 100 to form a percentage. For the 4.0-in base diameter case, the mean pitot pressure was 6.34 psia, and the RMS noise was 3.06%. For the 5.75-in. base diameter case, the mean pitot pressure was 6.40 psia, and the RMS noise was 4.43%. The RMS noise increases with base diameter, and is roughly 3 times larger than the freestream noise at this pressure. The agreement in the mean pitot pressure is sufficiently good to clearly indicate that even the 5.75-in. base-diameter cone did start. This is not unexpected, since the ratio of cone size to tunnel size is similar to that used in Mach-6 experiments at ITAM in Russia [27].

Slab Delta at 40-deg. Angle of Attack

Blockage tests were performed using 70-deg. swept slab-delta models that are 3/4-inch thick with a hemicylindrical leading edge and a hand-worked hemispherical tip. The models used for the tests ranged from 4 to 8 inches long. The driver-tube stagnation pressure was 120 psia for these cases, and the stagnation temperature was 160 deg. C. The model surface Kulite was located on the centerline behind the mounting point on the windward surface. A 250-psia Kulite was used for initial runs, but was replaced with a 15-psia stopped Kulite, in order to give more accurate results at the low pressures measured. Runs were performed both with and without a Pitot probe in the flow.

A LATCH computation was performed by Harris Hamilton at NASA Langley to predict the pressure on the surface of the blockage models. The value that is expected from this calculation is 2.07 psia for a Mach-6 freestream and a stagnation pressure of 120 psia. The measured pressure was always significantly higher than this. The pressure found on each model is noted in Table 1, as well as the location of the Kulite with respect to the leading edge and trailing edge. For all of the tests, the pressure fluctuations on both the model and the Pitot probe were much higher than expected. The model-surface pressure fluctuations ranged from 35% to 60% and the Pitot pressure fluctuations ranged from 25% to 60%. Since the pressures are lower than subsonic pressures, but not as low as expected, it is uncertain what is really occurring, and whether all or none of these models can be successfully tested in near-uniform Mach-6 flow. It may be that the bow shock from these blunt models is interacting with the nozzle-wall boundary-layer to cause major disturbances to the nominally-uniform flow. The authors are not aware of any other measurements of surface-pressure fluctuations on slab-delta models.

Status of Quiet-Flow Performance

The nozzle was designed using e^N theory following earlier work at Langley [17, 28, 18]; transition occurs much earlier than was predicted. Possible causes of the early transition on the nozzle wall include:

1. fluctuations generated at the nozzle throat due to problems with the bleed-slot flow
2. a nozzle-wall temperature distribution that decreases much more rapidly downstream than was initially expected
3. a 0.001-0.002-inch ($Re_k < 12$) rearward-facing step at the downstream end of the electroform [22]. Here, Re_k is a roughness Reynolds number based on the height of the peak roughness, and the conditions in a smooth-wall boundary layer at the roughness height.
4. the lack of polish on the downstream nozzle sections (although $Re_k < 12$)
5. some other problem (such as noise in the driver tube that doesn't show up in the low-noise pressure measurements made on the contraction wall)
6. some fundamental problem with the use of a very long nozzle which is not captured by the e^N analysis.

Item (1) has been the main suspect. Item (2) is expected to have an effect, but not sufficiently large to preclude quiet flow even at $Re \simeq 3\times10^5$/ft., our lowest operating condition so far. The Langley Mach-6 quiet tunnel was polished all the way to the end, so although items (3) and (4) treat roughness less than the $Re_k = 12$ criteria set by Beckwith, perhaps this roughness has a larger effect than expected when it is present in the very long nozzle. In particular, Görtler vortices can be induced by small roughness,

Model Length	Dist from LE to Kulite, in.	Dist from TE to Kulite, in.	Mean Pressure, psia
4 in.	3.5	0.5	3.12 to 4.28
5	4.15	0.85	2.35
6	4.75	1.25	2.66 to 3.1
7	5.5	1.5	2.59
8	6.15	1.85	2.60

Table 1: Pressure Measurements on Slab-Delta Blockage Models

so perhaps the roughness near the beginning of the concave-curvature section is much more critical than the $Re_k = 12$ criterion had led us to expect. Items (1)-(5) will have to be ruled out, before item (6) can be concluded. *Progress in the design and fabrication of quiet tunnels requires us to systematically address items (1) - (5).* If all correction efforts eventually failed, then we would have to conclude that the \$0.5m Mach-6 nozzle is not capable of providing high-Reynolds number quiet flow, in which case future progress in quiet-tunnel development would depend on determining why this is the case.

Effect of Changes in
Temperature Distribution of Nozzle

One approach towards obtaining quiet flow is to change the nozzle-wall temperature distribution. During the design and analysis of the nozzle contour, the wall temperature was assumed to drop linearly from 820 R at the throat to room temperature at section 8 [17].However, finite-element computations have shown that the temperature will drop to ambient in the first meter of the nozzle, and measurements have shown similar results [21]. Thus the effect of changing the nozzle-wall temperature distribution was investigated by insulating portions of the nozzle wall and contraction.

The experiments were carried out using the Case-5 throat geometry used previously, which exhibited no quiet flow [23]. Ceramic fiber insulation that was 1-1/2 inches thick was used. Two layers were used, since one layer was not enough to provide sufficient insulation. The pitot pressures and fluctuations were measured with the 0.062-in Kulite pitot probe on the centerline, $84.63 \pm 1/6$ in. downstream from the throat. The driver tube and contraction temperatures were set to 413 K for all the runs to be described, except for the last run which was set to 433 K. The initial driver-tube pressure for all runs was one atmosphere.

A baseline case was run first, with no insulation (Run 1). Since the tunnel had been cooled down, the tunnel was heated for 24 hours. From this point on,

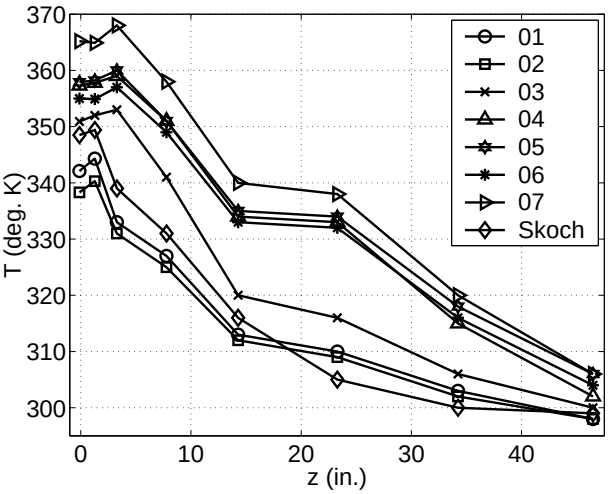

Figure 8: Temperature Distribution in Mach-6 Quiet Nozzle

insulation was added progressively, in the following regions in order: Run 2: throat (nozzle sections 1 and 2), Run 3: downstream portion of contraction, Run 4: nozzle sections 3 and 4, Run 5: nozzle section 5, Runs 6 and 7:the upstream portion of the contraction. Runs 6 and 7 have identical insulation configurations, only the upstream driver and contraction temperature was changed. Table 2 summarizes the runs.

The measured nozzle temperature distributions for all cases are shown in Figure 8. The first two data points correspond to the 2nd and 3rd thermocouples, which are positioned as shown by the crossed-circles in Figure 9. The origin of the z-axis is at the throat. The overall temperature increases as each section of insulation is added, as would be expected. The last case labeled 'Skoch' was measured previously, without insulation, with the tunnel heated to 433 K. Figure 10 shows the same data, normalized by the respective driver-tube temperature. This plot clearly shows that using the insulation raises the temperature significantly, although less than initially expected.

Run No.	Wait Time (hours)	Initial Driver Temperature (K)	Initial Driver Pressure (psia)	Pitot Noise Level (percent of mean)
1	24	413	14.477	5.7742
2	14	413	14.455	5.6658
3	25.5	413	14.547	5.5275
4	21	413	14.446	5.6918
5	18.5	413	14.527	5.5197
6	21.5	413	14.486	5.4695
7	12	433	14.407	5.2166

Table 2: Conditions and Resulting Noise Levels for Different Nozzle Wall Temperature Distributions

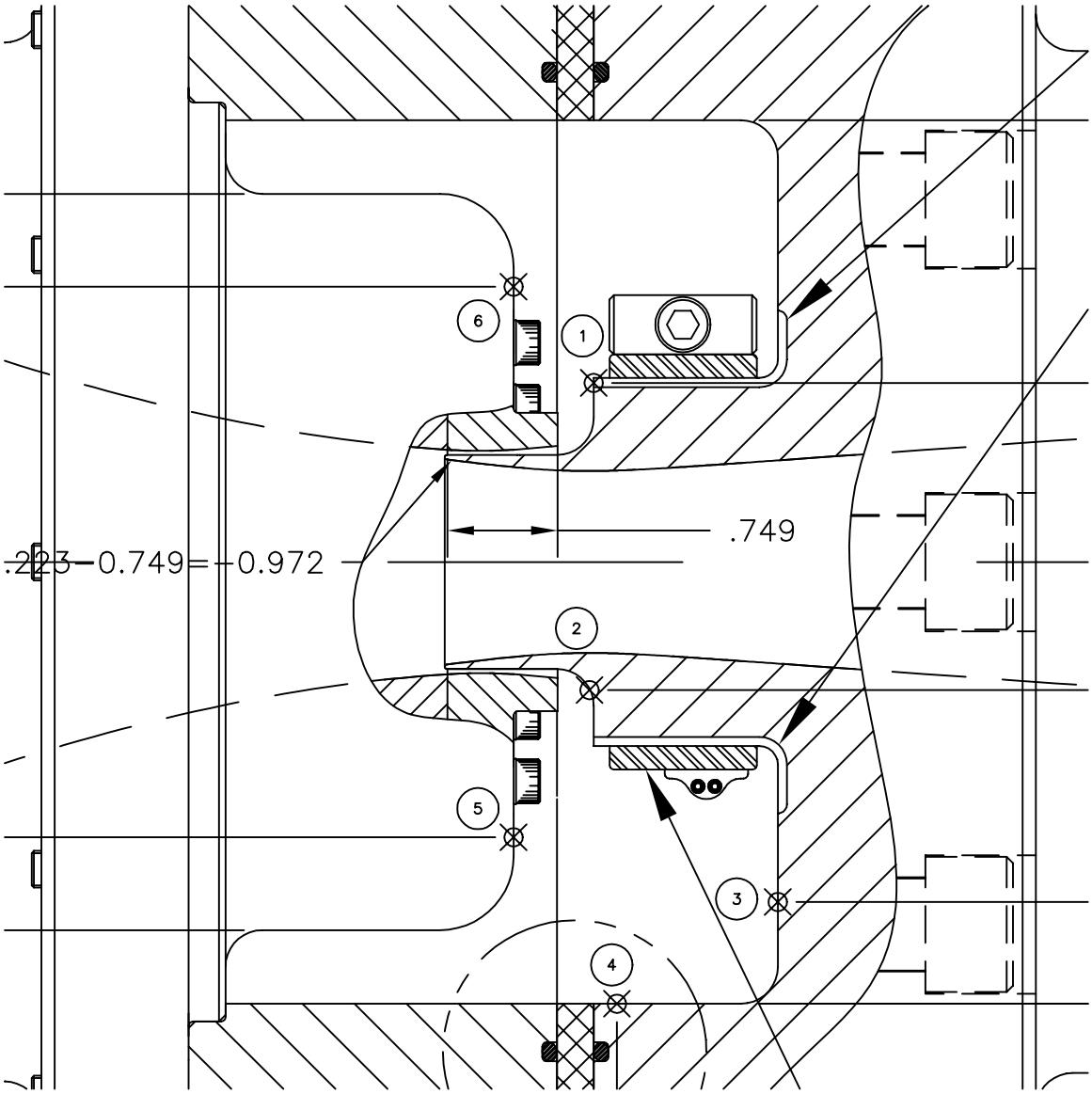

Figure 9: Drawing of Thermocouple Locations in Mach-6 Quiet Nozzle

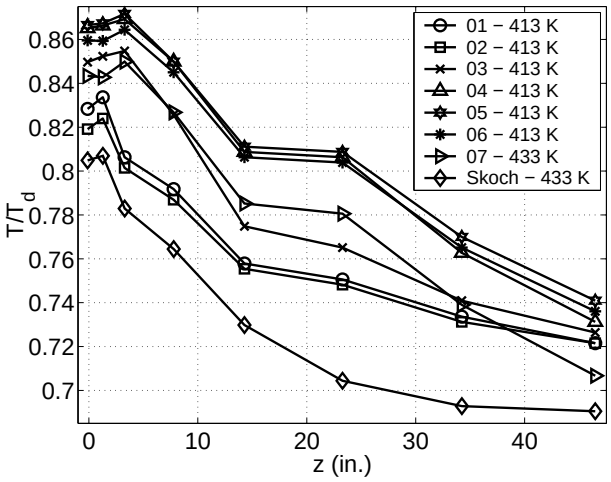

Figure 10: Normalized Temperature Distribution in Nozzle

Even though the temperature has increased overall, the plots show that the temperature still drops near ambient about 45 inches from the nozzle throat. This is only about 10 in. downstream of the uninsulated "Skoch" reference case. This shows that the insulation is not sufficient to make a large change in the temperature distribution of the nozzle. Heaters will need to be added, if a slower temperature drop along the nozzle is to be obtained.

The measured noise levels for each case are listed in Table 2. The noise level seems to decrease with the addition of more insulation, except for Run 4. This is probably because the change in wall temperature changes the boundary-layer properties. Comparing to the previous section on the effects of driver-tube temperature, note that a warmer nozzle-wall temperature or a colder driver-tube-gas temperature both lower the pitot fluctuations, which seems consistent.

Design of the Sixth Throat-Region Bleed-Slot Geometry

Problems with the bleed-slot flow have been the primary suspect for the cause of the lack of quiet flow. These could include: (1) unsteady massflow in the slot, (2) incorrect massflow, so that the nozzle-wall boundary layer separates from the bleed lip, with the resulting separation bubble causing early transition [29], or (3) insufficient massflow in the slot, causing contraction-wall turbulence to slip past into the nozzle. The bleed-slot throat design was modified to facilitate iterative changes in the geometry, and tests with five different geometries were reported in Jan. 2002 [23]. A sixth bleed-slot geometry was designed and fabricated in Spring 2002, with results reported here.

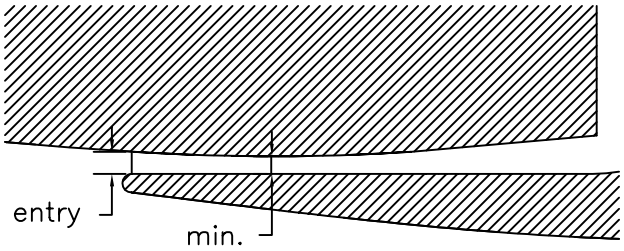

Figure 11: Detail Defining Critical Dimensions of Slot Throat

Fig. 11 shows a generic detail of the slot itself, taken from Ref. [23]. The height of the upper wall above the top of the bleed-lip tip is defined as 'entry', and the minimum height of the slot is defined as 'min.' These parameters are provided in Table 3 for all the cases tested so far; this table is updated from Tables 1 and 4 in Ref. [23].

A critical part of the suction-slot design is achieving a separation streamline that attaches smoothly to the tip of the bleed lip, toward the main-flow side, so that a separation bubble is avoided in the nozzle-wall boundary layer. One way to think of this design problem is in terms of matching the pressures on both sides of the separation streamline, at the entry to the slot. To do this, Beckwith and Chen used the one-dimensional (1D) method of streamtubes (Ref. [30], and private communications with Frank Chen and Ivan Beckwith, NASA Langley, 1990-2002). Although the complete procedure used by Beckwith can no longer be determined, the new Case-6 design described here attempted to follow it more closely than before.

The use of the streamtube method is supported by our previous measurements [23, p. 12], especially for Case 4, which showed that the pressure in the slot at the transducer can be predicted with fair accuracy using a 1D inviscid analysis. The measured pressures are only a few percent high or low, perhaps due to viscous effects or experimental error. This suggests that Beckwith's method of streamtubes should have reasonable accuracy.

Beckwith and Chen used a Hopkins-Hill solution for the throat region to obtain the main-flow side of the bleed-lip geometry; this procedure was also followed in the present design [18]. The Hopkins-Hill solution used to design the bleed lip shape can be used to determine $P_e/P_t = 0.8225$ and $M_e = 0.537$ at the beginning of the lip, on the main flow side, at the joint between the hemispherical tip and the

inner contour. Here, P_e is the local static pressure, P_t is the stagnation pressure, and M_e is the local Mach number.

There is an error on page 12 of Ref. [23] in the right-hand column, which refers to $M_e = 0.66$ and $P_e/P_t = 0.75$ from a 1D solution. This computation was wrong, since it used the radius ratio as an area ratio, instead of using the radius ratio squared. The nozzle throat radius is 0.6178 inches, and the radius of the bleed lip at the hemisphere junction is 0.6963 in. This results in an area ratio of 1.2703, so that a 1D inviscid analysis results in $M_e = 0.54$ and $P_e/P_t = 0.82$. This nearly matches the Hopkins-Hill solution, confirming that the gentle throat geometry is nearly one-dimensional.

The slot entry and slot minimum dimensions can then be used to correct Table 4 of Ref. [23], as shown in Table 3 below. Note that the height ratio 'entry'/'min.' is taken as the area ratio A_{entry}/A^* in the annular slot, although this is not true in the main flow. Using this area ratio in the slot, the pressure at the slot entrance, P_{se}, can be computed as a ratio to P_t, assuming sonic flow at the slot minimum. Here, the slot entrance is taken to be the junction between the hemispherical tip and the upper surface of the bleed lip. This is again a 1D analysis in the slot, and this analysis also neglects the 0.030-in.-dia. bluntness of the bleed lip tip.

One can then examine P_{se}/P_t for the various designs. Since P_e/P_t on the main flow side of the lip is about 0.82, case 4 couldn't work, since the higher pressure on the slot side would cause a separation bubble on the main-flow side. One still might expect that Cases 1, 2, 3, and 5 could work, but the flow remained noisy. Perhaps the pressure on the slot side should be a bit lower, as in case 5, to pull more flow into the slot. The pressure was low for Case 3, but this geometry placed the slot throat very near the bleed lip, so it may have caused other problems.

To address this question, $h_e(P_e/P_t = 0.82)$ was computed. This is the slot entry height for which $P_{se}/P_t = 0.82$, matching the main-flow side (again neglecting the 0.030-inch tip). How far from below the top of the bleed lip does the slot draw, again assuming 1D flow, and assuming the pressure at the main-flow side of the tip is unchanged? For $P_{se}/P_t = 0.82, A_e/A^* = 1.27$. Here, A_e is the flow area at the entrance of the lip, and A^* is the sonic-flow area in the suction slot. This leads to the computation of $h_{e,tip}$, the height from the top of the tip (which is 0.030-inch thick) at which the separation streamline is nominally located. This should be at least half the height of the tip, or at least 0.015 inches, and preferably more like 0.020 or 0.025 in. This resulted in the design of Case 6. It is very interesting to note that if there isn't enough suction, then there isn't enough area ratio available to draw much from the bleed lip tip (cp. cases 3 and 6).

Case 6 sucks 30% of the massflow through the slot, about 3 times more than in the original design, for a height at the lip entrance of 0.1088 inches. It was also noted that the conical convergence of the upper side of the slot used in Cases 4 and 5, combined with the cylindrical lower side, means that flow was converging coming into the minimum. This, combined with the previous use of a sharp edge at the minimum, will have caused the minimum height at the sonic point to be less than the geometrical minimum, since the flow will continue to contract until the flow turns. This might also have been causing fluctuations in the massflow, as the actual sonic minimum is past the geometrical edge. For Case 6, a smooth matched circular arc with a 1.68-inch radius was thus added, to bring the conical convergence to a parallel flow; it was followed by a 0.25-in. radius on the diverging section, which seems similar to the values used by Beckwith and Chen.

The Case 6 design seeks to draw flow in from about 2/3 of the way down from the top of lip (again, using a 1D analysis, and assuming that the pressure on the main-flow side remains unchanged). This requires picking up the separation streamtube at about 0.020-in. from top of lip. The streamtube entrance height is then really 0.1088+0.020 or 0.1288. If $P_e/P_0 = 0.82$ here, to match the nominal lower pressure, then $A/A^* = 1.27$, and the height at the slot minimum should be 0.1014. The nominal P_{se}/P_t based on the height above the lip is then 0.70, using $A/A^* = 0.1088/0.1014 = 1.073$. Note that this is now the first design to draw from below the middle of the bleed-lip tip, using this 1D streamtube analysis. Note also that the tip thickness is now becoming fairly small compared to the slot width.

It was also noted that the Beckwith bleed-lip designs have a much larger angle with respect to contraction wall, so the angle was increased by 1.6 degrees for Case 6, which was as much as was possible with the present geometry while maintaining monotonic slopes in the contraction contour. Fig. 12 shows the modification to the geometry. The horizontal axis, z', is the axial contraction coordinate, where $z' = 0$ at the contraction entrance. The modifications were made to an insert that picks up the contour at $z' = 37.0$ in. The contour again makes a smooth joint at the match point, with a larger radius downstream, and with the difference in radius

Case:	1	2	3	4	5	6
entry, in.	0.036	0.036	0.036	0.073	0.073	0.1088
min. in.	0.029	0.029	0.036	0.042	0.062	0.1014
A_{entry}/A^*	1.24	1.24	1.0	1.74	1.18	1.073
P_{se}/P_t	0.81	0.81	0.53	0.91	0.78	0.70
$h_e(P_e/P_t = 0.82)$, in.	0.037	0.037	0.046	0.053	0.079	0.1288
$h_{e,tip}(0.82)$, in.	0.001	0.001	0.010	-0.020	0.006	0.020

Table 3: Properties of Bleed-Slot Geometries

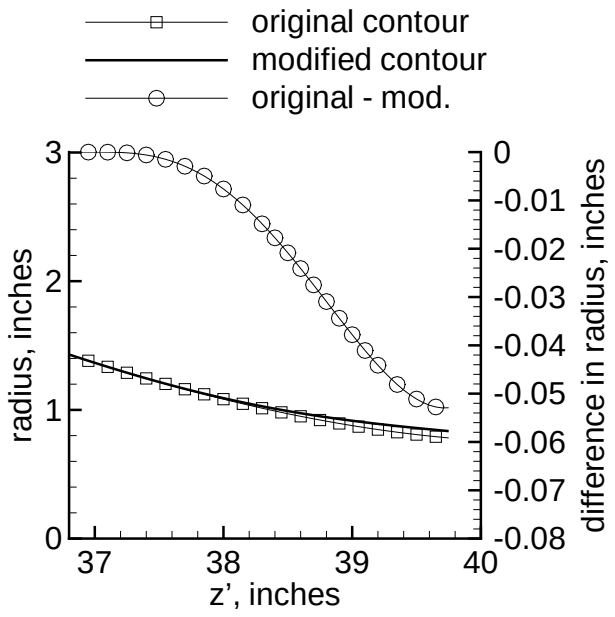

Figure 12: Modification to Contraction Contour, Case 6

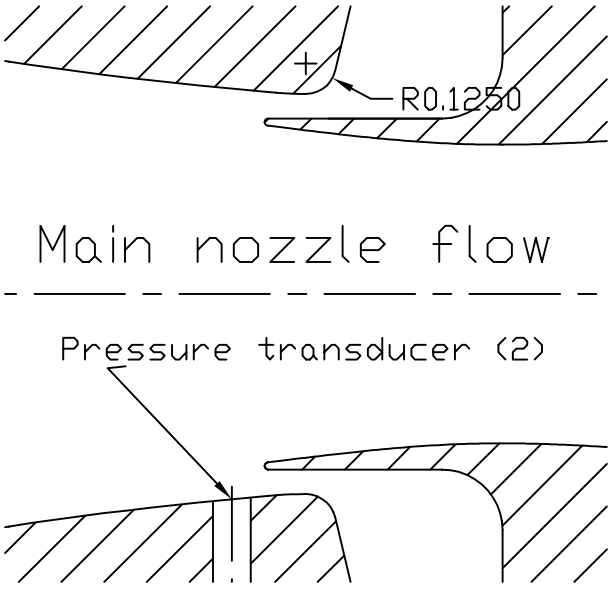

Figure 13: Drawing of Slot Throat, Case 6

increasing monotonically.

Fig. 13 shows a drawing of the new geometry. The dimension is in inches. The upstream joint with the stainless-steel contraction section is nearly flush on the bottom surface, but contains a forward-facing step on the upper side of between 0.001 and 0.002 inches (as estimated by a skilled machinist).

Mean Flow and Noise Measurements Using the Sixth Geometry

Although the sixth throat geometry did not result in high Reynolds number quiet flow, the increased suction-slot massflow seems to have reduced the tunnel runtime only slightly, from about 10 sec. to about 9 sec., and it has enabled us to obtain some initial quiet flow at very low pressures. Figures 14 and 15 show turbulent spots dropping out to quiet flow as the stagnation pressure decreases during a run. The average driver tube stagnation pressure during the time of this plot is 7.785 psia, as measured by a static-pressure transducer near the en-

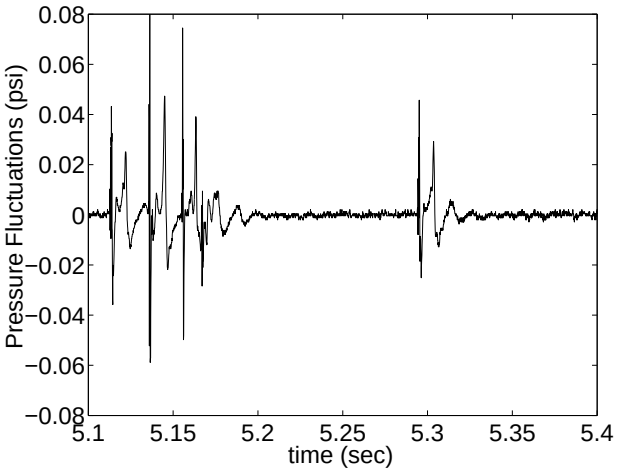

Figure 14: Pitot Fluctuations on Tunnel Centerline at $z = 84.3$ in.

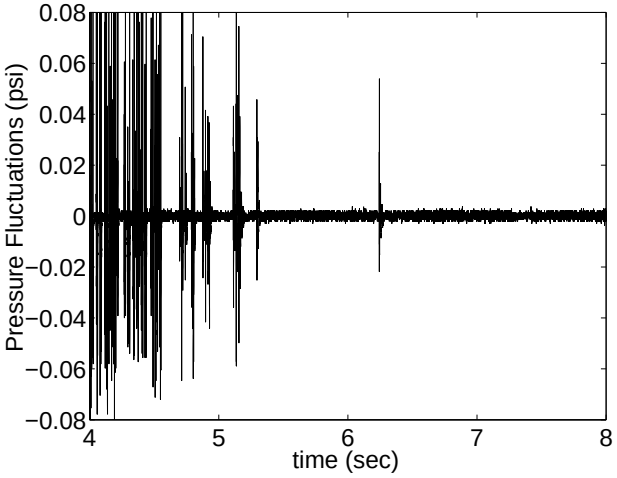

Figure 15: Pitot Fluctuations on Tunnel Centerline at $z = 84.3$ in., Longer Record

trance to the contraction, and the driver-tube temperature is 160 degrees C. Fully quiet flow occurs when the driver-tube stagnation pressure drops to about 7.5 psia. The Kulite pressure transducer near the beginning of the contraction is an XCE-080-250A model, with a maximum range of 250 psia, so it is not accurate at low pressures. The pitot Kulite is another 0-15 psia stopped model, with a 0.062-in. diameter. The signal was sampled at 500 kHz, using an 8-bit LeCroy oscilloscope.

The noise level during quiet flow was found by taking the RMS of the pressure fluctuations over a 0.3-second period, between 5.7 and 6.0 sec. after the start of the run. This was chosen because it was the longest duration of quiet flow for which data was acquired at high resolution and high sampling rates. The pre-run noise was found using the same length of record. The square root of the difference of the squares is used to find the corrected quiet-flow noise levels. These were then nondimensionalized by the mean pitot pressure during the time period to result in a noise level of 0.15%; the value based on the uncorrected pitot fluctuations would be 0.2%, so the signal/noise ratio is about 4. Although this is higher than the 0.1% nominal limit for quiet flow, the disappearance of the turbulent-spot signatures with decreasing pressure clearly indicates the presence of nearly quiet flow. Data at this high resolution presently exists only at this pressure, so comparisons to other pressures cannot yet be made.

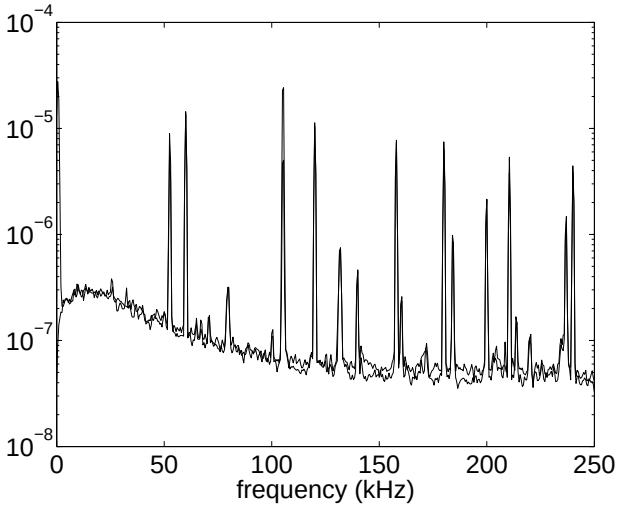

Figure 16: Power Spectra of Pitot Fluctuations at $z = 84.3$ in.

To see if the RMS was changing during the lower-noise period, this time was divided up into 0.01-sec. periods and the RMS was found for each. The pitot fluctuations scatter from 0.17% to 0.26% of the mean, apparently randomly. The signal/noise ratio may not be sufficient to get good resolution from these records.

Power spectra of the quiet-flow noise and the pre-run noise are shown in Figure 16 using a window length of 1000 points, or 2 ms. The vertical scale is not yet calibrated. These correspond well, indicating that a large percentage of the noise captured is background electrical noise. The only place where the spectra differ greatly is at low frequencies. Figure 17 shows this more clearly, where a window length of 30000 points, or 60 ms, was used to better capture the lower frequencies.

The quiet flow was examined with the Pitot

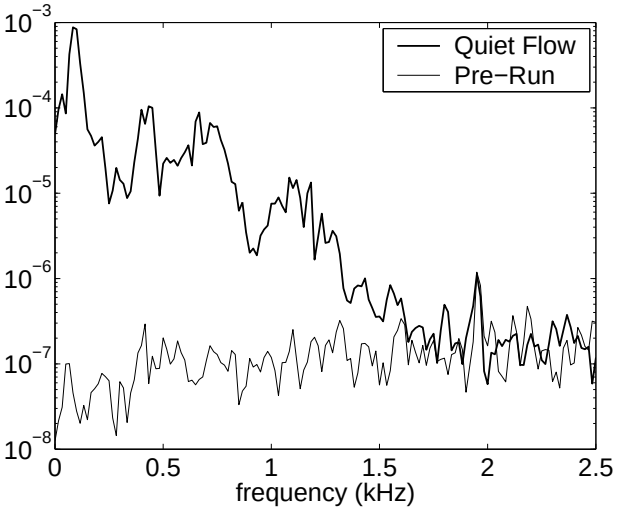

Figure 17: Low-Frequency Power Spectra of Pitot Fluctuations at $z = 84.3$ in.

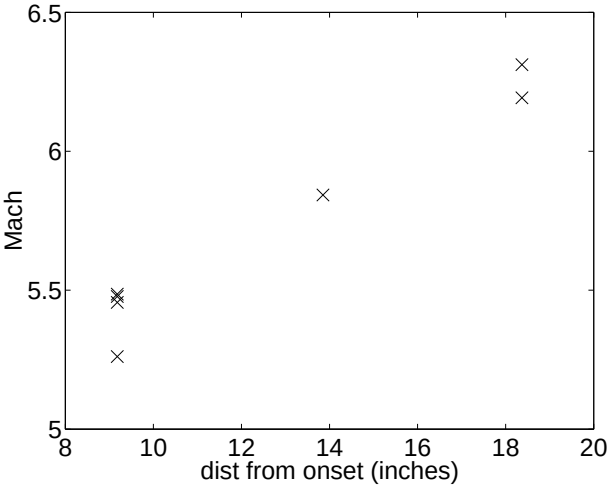

Figure 18: Preliminary Measurements of Axial Mach Number Variation in Quiet Flow Area

probe at the front, middle, and back of the present axial range. The Mach numbers are shown in Figure 18. The horizontal axis is the distance from the nominal onset of uniform flow. These preliminary measurements show that the Mach number still seems to be increasing beyond where it is expected to be uniform. The unit Reynolds numbers range from over 200,000/ft at the front to 150,000/ft at the back. These unit Reynolds numbers were computed by obtaining the Mach number using the Rayleigh pitot formula, and the measured contraction-wall total pressure and pitot pressure. Isentropic theory was used to compute the static temperature and density. This apparent nonuniformity remains under investigation.

The intermittency was calculated throughout the run using a second derivative method similar to that used in Ref. [31]. This is calculated from data taken at 10 kHz for the entire run. These records are digitized rather too slowly to obtain reliable RMS pitot pressures. The flow may be considered quiet when the intermittency is below 1%. The intermittency is plotted in Figure 19 for 7 runs performed at nearly the same initial conditions, at 3 probe locations. This is plotted for data taken with the pitot probe placed on the centerline in the forward, middle and aft parts of the testing area, which corresponds to 9.18, 13.85, and 18.37 inches, respectively, beyond the nominal onset of uniform flow (which is at $z = 75.12$ in., where $z = 0$ at the nozzle throat). The figure shows the flow becoming quiet at nearly the same driver tube pressure over a large area, which could indicate that once the pressure becomes low

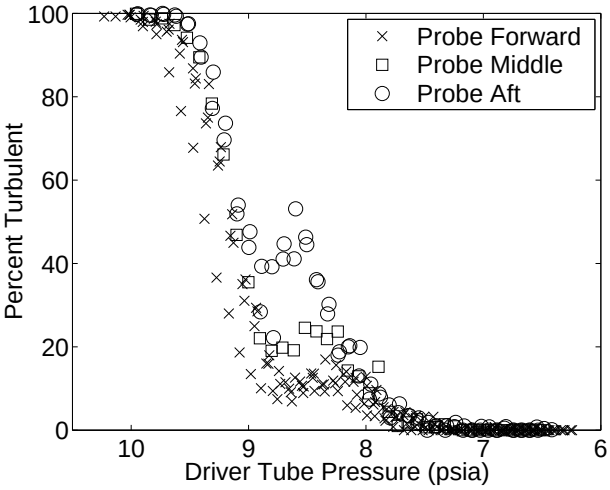

Figure 19: Intermittency of Pitot Measurements in Near-Quiet Flow

enough, all of the flow becomes quiet. This differs from what is usually observed, where the onset of turbulence would move downstream as the pressure decreases.

Plans for Improving Quiet-Flow Performance

It appears that the Case-6 slot geometry, with increased suction massflow, has provided some quiet flow for the first time. Since the runtime did not decrease markedly, and the pressure in the suction plenum remains low (not shown here), further modifications in the suction geometry are to be attempted.

In addition, the step at the end of the electroform is now suspect, along with the 30 microinch RMS finish on most of the nozzle, including the possibly crucial region near the end of the radial flow section, where Görtler vortices originate. Current plans call for disassembling the nozzle and having most of the nozzle length polished, to better approximate the finish in the Langley Mach-6 quiet nozzle.

Preliminary TSP Measurements on the Hyper2000

Temperature sensitive paint (TSP) has been shown to be a useful technique for studying stationary streamwise vortices, which are one possible form of instability leading to transition [32, 33].The technique is being applied to a Hyper-2000 (H2000) model. The H2000 is a publically releasable geometry that is generic for the Hyper-X class of vehicles [34]. The two geometries appear to be identical along the centerplane.

The general TSP technique is documented in several excellent references such as Refs. [35, 36, 37]. The experimental technique and image processing developed specifically for the BAM6QT is documented in Ref. [33]. Two major changes have been made to the technique since then. First, a larger 4-in. blue LED array (ISSI LM4 464nm) is now used for exciting the paint layer. Compared to the 2-in. LM2 model, this outputs more light, resulting in a higher signal-to-noise ratio and better uniformity of the lighting. Second, Dichlorotris(1,10-phenanthroline) ruthenium(II) hydrate (or Ru(phen) for short) is used now for the luminophore, as suggested in [38]. The calibration of this luminophore against Ru(bpy), the luminophore used in Refs. [32, 33], is shown in Figure 20. Ru(phen) shows a slightly higher sensitivity in the temperature range of interest, above 300 K. This calibration was done using the same blue LED and CCD camera (Photometrics Sensys 0401E) used for the wind tunnel testing.

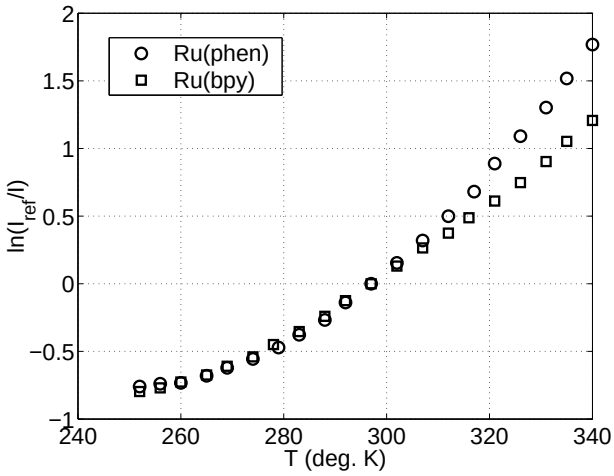

Figure 20: Calibration of Two Luminophores

Run	P_0 (psia)	T_0 (deg. R)	LE Configuration
1	109.3	751	Smooth
3	111.7	754	Smooth
7	117.6	760	0.008-in. tape
8	117.8	767	0.008-in. tape

Table 4: Hyper2000 Test Conditions

Images from four tunnel runs will be presented. The flow conditions for each are listed in Table 4. For runs 7 and 8, strips of metallic tape 0.1 inches wide and 0.008 inches thick were taped around the leading edge to generate stronger streamwise vortices. The disturbances are presently measurable only well downstream of the tapes. This repeatable technique for introducing disturbances was adapted from Ref. [39], and allows controlling the downstream disturbances by varying the height and spacing of the roughness elements. The concept is adapted from the low-speed crossflow work of Saric et al. [40], where it has been very productive.

The images taken during the run are converted into a temperature map by applying the calibration shown in Figure 20. The temperatures are then converted into heat transfer rates using a simple one-dimensional heat-conduction model, in which the insulator thickness is assumed constant and the underlying model temperature is assumed to remain at the pre-run value. The values are normalized by an arbitrary point on the image [41]. This process factors out the thermal conductivity and thickness of the paint, which are two values that are not accurately

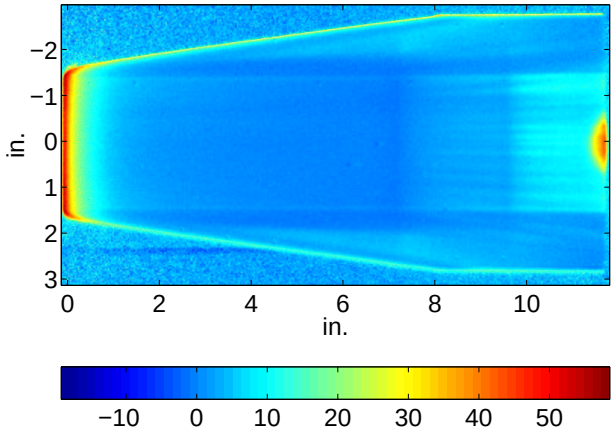

Figure 21: q/q_{ref} for Smooth H2000, Run 1

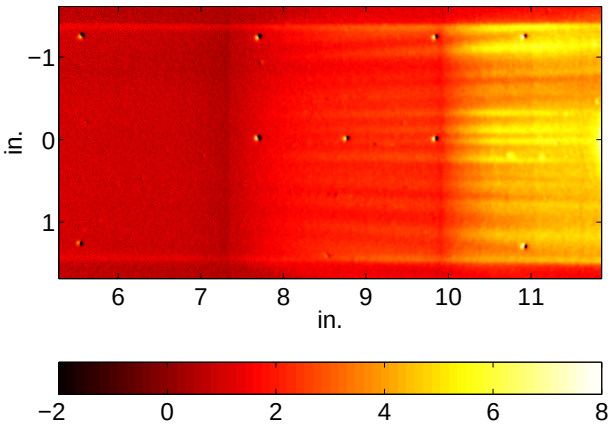

Figure 22: q/q_{ref} for Smooth H2000, Run 3

known at present.

Figure 21 shows the result from run 1. For all the images, the origin of the horizontal axis is at the leading edge, and the origin of the vertical axis is at the centerline. Also, the color scale extends down to a negative value, which would suggest heat transfer from the model to the flow. However this is not the case anywhere on the model, and the scale is set this way only because the image processing software produced a clearer image of the weak vortices. The high heating at the thin leading edge is clearly seen. The heating rate quickly decreases as the laminar boundary layer thickens downstream. Streak marks can be seen starting to develop on the second ramp, past the first corner, which is at about 7-1/3 inches, and has a 5.5-deg. compression angle. The streaks seem to grow after passing through the second compression corner, which is located near 10 inches, and compresses by 3 degrees. These streak marks are probably streamwise vortices that are generated by the small imperfections in the leading edge and by the roughness of the paint finish (cp. Refs. [39], [42], and [43]). There is a curious high-heating area at the trailing edge of the model near the centerline. Although this might be a sign of onset of turbulent flow, it may also be caused by a shadow of some sort from the lighting. In principal, shadows should not appear in these images, since they should show up in the wind-off and wind-on images, and be ratioed out during the image processing. However, this shadow was seen for all the runs, regardless of the camera location. The exact cause of the shadow will be determined during future experiments.

Figure 22 shows a closer view of the compression corners. The streaks caused by the vortices can be seen much more clearly in this image. The nine dots

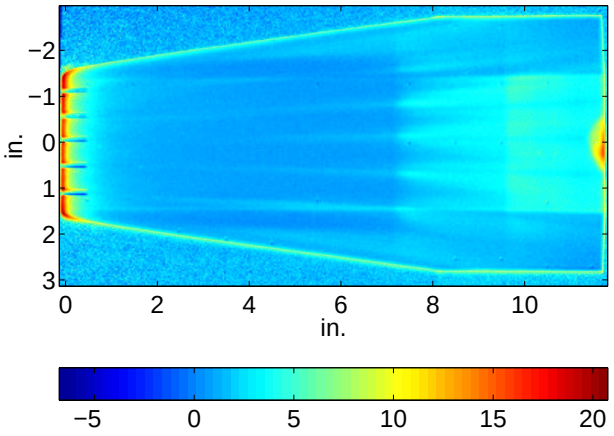

Figure 23: q/q_{ref} for H2000 with L.E. Roughness, Run 7

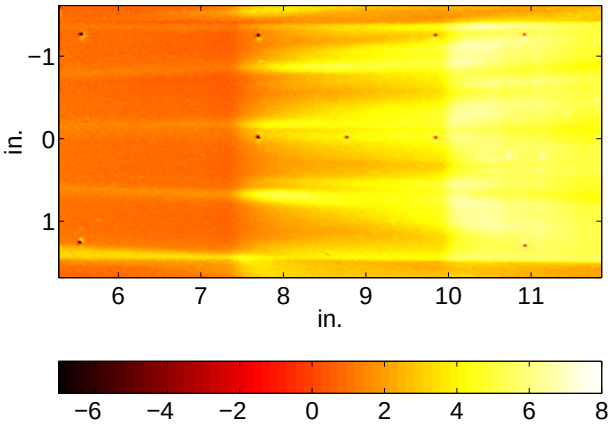

Figure 24: q/q_{ref} for H2000 with Leading Edge Roughness, Run 8

are registration marks used for mapping the image to a grid. Because the camera was positioned much closer to the model for this run, the model moved much more with respect to the camera than in the previous case, and it was more difficult to align the wind-off and wind-on images.

Figure 23 shows the results from run 7, in which the H2000 has strips of tape wrapped around the leading edge. Five strips were used; they can be clearly seen in the image. The streamwise vortices generated by them become clearly visible about 4-6 inches downstream from the leading edge. The vortices from the three inner strips stay on the three ramps, but the outer two get swept away onto the chine, apparently due to an outer-directed crossflow. This same outer-directed crossflow can be seen in Ref. [34]. A slight outer curvature in the inner three vortices can be seen as well. These three vortices seem to break down rapidly once they pass through the compression corners.

This is more clearly seen in Figure 24. The three vortices can be seen approaching the first compression corner. The high-heating streaks rapidly spread out on the second ramp, leaving apparently undisturbed flow in between. This may be an indication of transition. After the second compression corner the streaks seem to merge together, which would again suggest the onset of turbulent flow. Hot- wire measurements will be performed to determine the character of the flow in these regions.

Summary

Purdue University continues to develop the 9.5-inch Mach-6 Boeing/AFOSR Mach-6 Quiet Tunnel. A sixth bleed-slot-throat geometry was partially successful, for initial quiet flow was achieved at very low Reynolds numbers of about 200,000. Work continues towards modifying the nozzle to achieve high Reynolds number quiet flow.

Measurements of the pitot fluctuations in the nozzle at higher Reynolds numbers, with a turbulent boundary layer, show a reduction in noise of a factor of 4 as the driver-tube temperature is reduced from $180°C$ to $20°C$. This suggests that conventional-tunnel measurements of transition location will be influenced not only by unit Reynolds number but also by tunnel-wall temperature ratio, since the radiated noise level in the tunnel appears to depend on both factors.

Development of instrumentation also continues. Hot wires with a relatively low length/diameter ratio of 100 have been fabricated and have survived many tunnel runs. Galling problems in the automated vertical traverse system have been addressed by design modifications.

Initial measurements have also been made on a Hyper2000 model, which is generic for the Hyper-X class of vehicles. Temperature-sensitive paint measurements show the development of streamwise vortices downstream of imperfections in the leading edge; these streamwise vortices grow rapidly in the compression corners, and provide one possible mechanism for transition in this geometry. Initial controlled measurements are reported, using small roughness tapes wrapped around the leading edge, ala Ginoux. These techniques now provide a method for detailed study of the streamwise-vortex transition mechanism.

Acknowledgements

The research is funded by AFOSR under grant F49620-00-1-0016, by Sandia National Laboratory under contracts BG-7114 and 3248, and by NASA Langley, under grant NAG1-01-027. Additional support is being provided by a partial graduate-student fellowship from TRW, and by grant NAG-9-1385 from NASA Johnson. Frank Chen and Steve Wilkinson from NASA Langley continued to provide assistance in making the best possible use of information available from the earlier NASA Langley quiet-tunnel development effort.

REFERENCES

[1] Scott A. Berry, Thomas J. Horvath, Brian R. Hollis, Richard A. Thompson, and H. Harris Hamilton II. X-33 hypersonic boundary layer transition. Paper 99-3560, AIAA, June 1999.

[2] H.A. Korejwo and M.S. Holden. Ground test facilities for aerothermal and aero-optical evaluation of hypersonic interceptors. Paper 92-1074, AIAA, February 1992.

[3] AGARD, editor. *Sustained Hypersonic Flight*. AGARD, April 1997. CP-600, vol. 3.

[4] Tony C. Lin, Wallis R. Grabowsky, and Kevin E. Yelmgren. The search for optimum configurations for re-entry vehicles. *J. of Spacecraft and Rockets*, 21(2):142–149, March-April 1984.

[5] I.E. Beckwith and C.G. Miller III. Aerothermodynamics and transition in high-speed wind tunnels at NASA Langley. *Annual Review of Fluid Mechanics*, 22:419–439, 1990.

[6] Steven P. Schneider. Effects of high-speed tunnel noise on laminar-turbulent transition. *Journal of Spacecraft and Rockets*, 38(3):323–333, May–June 2001.

[7] Steven P. Schneider. Flight data for boundary-layer transition at hypersonic and supersonic speeds. *Journal of Spacecraft and Rockets*, 36(1):8–20, 1999.

[8] F.-J. Chen, M.R. Malik, and I.E. Beckwith. Boundary-layer transition on a cone and flat plate at Mach 3.5. *AIAA Journal*, 27(6):687–693, 1989.

[9] S. P. Wilkinson, S. G. Anders, and F.-J. Chen. Status of Langley quiet flow facility developments. Paper 94-2498, AIAA, June 1994.

[10] I. Beckwith, T. Creel, F. Chen, and J. Kendall. Freestream noise and transition measurements on a cone in a Mach-3.5 pilot low-disturbance tunnel. Technical Paper 2180, NASA, 1983.

[11] Alan E. Blanchard, Jason T. Lachowicz, and Stephen P. Wilkinson. NASA Langley Mach 6 quiet wind-tunnel performance. *AIAA Journal*, 35(1):23–28, January 1997.

[12] S. P. Schneider and C. E. Haven. Quiet-flow Ludwieg tube for high-speed transition research. *AIAA Journal*, 33(4):688–693, April 1995.

[13] Steven P. Schneider, Steven H. Collicott, J.D. Schmisseur, Dale Ladoon, Laura A. Randall, Scott E. Munro, and T.R. Salyer. Laminar-turbulent transition research in the Purdue Mach-4 quiet-flow Ludwieg tube. Paper 96-2191, AIAA, June 1996.

[14] J.D. Schmisseur, Steven H. Collicott, and Steven P. Schneider. Laser-generated localized freestream perturbations in supersonic and hypersonic flows. *AIAA Journal*, 38(4):666–671, April 2000.

[15] Terry R. Salyer, Steven H. Collicott, and Steven P. Schneider. Feedback stabilized laser differential interferometry for supersonic blunt body receptivity experiments. Paper 2000-0416, AIAA, January 2000.

[16] Dale W. Ladoon and Steven P. Schneider. Measurements of controlled wave packets at Mach 4 on a cone at angle of attack. Paper 98-0436, AIAA, January 1998.

[17] Steven P. Schneider. Design of a Mach-6 quiet-flow wind-tunnel nozzle using the e**N method for transition estimation. Paper 98-0547, AIAA, January 1998.

[18] Steven P. Schneider. Design and fabrication of a 9-inch Mach-6 quiet-flow Ludwieg tube. Paper 98-2511, AIAA, June 1998.

[19] Steven P. Schneider. Fabrication and testing of the Purdue Mach-6 quiet-flow Ludwieg tube. Paper 2000-0295, AIAA, January 2000.

[20] Steven P. Schneider. Initial shakedown of the Purdue Mach-6 quiet-flow Ludwieg tube. Paper 2000-2592, AIAA, June 2000.

[21] Steven P. Schneider, Shann Rufer, Laura Randall, and Craig Skoch. Shakedown of the Purdue Mach-6 quiet-flow Ludwieg tube. Paper 2001-0457, AIAA, January 2001.

[22] Steven P. Schneider and Craig Skoch. Mean flow and noise measurements in the Purdue Mach-6 quiet-flow Ludwieg tube. Paper 2001-2778, AIAA, June 2001.

[23] Steven P. Schneider, Craig Skoch, Shann Rufer, Shin Matsumura, and Erick Swanson. Transition research in the Boeing/AFOSR Mach-6 quiet tunnel. Paper 2002-0302, AIAA, January 2002.

[24] S.W. Kwon and Steven P. Schneider. Stress analysis for the window of the Purdue Mach-6 quiet-flow Ludwieg tube. Paper 2002-0309, AIAA, January 2002.

[25] John Laufer. Some statistical properties of the pressure field radiated by a turbulent boundary layer. *Physics of Fluids*, 7(8):1191–1197, August 1964.

[26] S.R. Pate and C.J. Schueler. Radiated aerodynamic noise effects on boundary-layer transition in supersonic and hypersonic wind tunnels. *AIAA Journal*, 7(3):450–457, March 1969.

[27] A.A. Maslov. Experimental study of stability and transition of hypersonic boundary layer around blunted cone. Technical report, Institute of Theoretical and Applied Mechanics,

Russian Academy of Sciences, Siberian Branch, Novosibirsk, Russia, December 2001. Final Technical Report, International Science and Technology Center Grant 1863-2000. Funded by the European Office of Aerospace Research and Development, U.S.A.F.

[28] Steven P. Schneider. Laminar-flow design for a Mach-6 quiet-flow wind tunnel nozzle. *Current Science*, 79(6):790–799, 25 September 2000.

[29] C. Quelin, S. Petit, and J. Delery. Etude au tunnel hydrodynamique TH1 du fonctionnement de la fente d'aspiration du collecteur de la soufflerie silencieuse R1Ch. Rapport Technique RT 1/03472 DMAE/DAFE, ONERA, Octobre 2000. In French.

[30] Timothy Alcenius, S.P. Schneider, Ivan E. Beckwith, and John J. Korte. Development of square nozzles for high-speed low-disturbance wind tunnels. Paper 94-2578, AIAA, June 1994.

[31] T. Hedley and J. Keffer. Turbulent/non-turbulent decisions in an intermittent flow. *Journal of Fluid Mechanics*, 64(4):625–644, 1974.

[32] S. Matsumura, C. Huang, Y. Choi, E.O. Swanson, T.R. Salyer, and T. Sakaue. Feasibility of detecting streamwise vortices from roughness elements using temperature sensitive paint in a Mach-4 ludwieg tube. Paper 2002-3238, AIAA, June 2002.

[33] S. Matsumura. Development of temperature-sensitve-paint technique for high-speed transition research in the Boeing/AFOSR Mach-6 quiet tunnel. Submittted to the AIAA Ground Testing Student Competition, 2002.

[34] Scott Berry, Aaron Auslender, Arthur D. Dilley, and John Calleja. Hypersonic boundary-layer trip development for Hyper-X. Paper 2000-4012, AIAA, August 2000.

[35] B.T. Campbell, T. Liu, and J.P. Sullivan. Temperature sensitive fluorescent paint systems. Paper 94-2483, AIAA, June 1994.

[36] M. Hamner. Demystifying luminescent paint technology: A guide for non-developers. Paper 2001-2981, AIAA, June 2001.

[37] T. Liu, B.T. Campbell, S.P. Burns, and J.P. Sullivan. Temperature- and pressure-sensitive luminescent paints in aerodynamics. *Applied Mechanics Review*, 50(4):227–246, April 1997.

[38] J.P. Hubner, B.F. Carroll, and K.S. Schanze. Heat transfer measurements in hypersonic flow using luminescent coating techniques. Paper 2002-0741, AIAA, January 2002.

[39] J.J. Ginoux. *Streamwise Vortices in Laminar Flow*, pages 395–422. AGARD, 1965. AGARDograph 97.

[40] R.H. Radeztsky, M.S. Reibert, and W.S. Saric. Effect of isolated micron-sized roughness on transition in swept-wing flows. *AIAA J.*, 37(11):1370–1377, November 1999.

[41] T. Liu, B.T. Campbell, and J.P. Sullivan. Fluorescent paint for measurement of heat transfer in shock-turbulent boundary layer interaction. *Experimental Thermal and Fluid Science*, 10(1):101–112, January 1995.

[42] Jean Ginoux. Streamwise vortices in reattaching high-speed flows: a suggested approach. *AIAA Journal*, 9(4):759–760, April 1971.

[43] Luigi de Luca, Gennaro Cardone, Dominique Chevalerie, and Alain Fonteneau. Viscous interaction phenomena in hypersonic wedge flow. *AIAA Journal*, 33(12):2293–2299, December 1995.